Contemporary Mathematics
https://ojs.wiserpub.com/index.php/CM/

Research Article

# The Block Arithmetic Mean Iterative Method for Solving Radiation Transport Model

**Mohana Sundaram Muthuvalu[1*], Mathiyalagan Kalidass[2], M. Sambath[3], Shaher Momani[4,5]**

[1]Department of Applied Science, Universiti Teknologi PETRONAS, Perak, Malaysia
[2]Department of Mathematics, Bharathiar University, Coimbatore, India
[3]Department of Mathematics, Periyar University, Salem, India
[4]Department of Mathematics, The University of Jordan, Amman, Jordan
[5]Nonlinear Dynamics Research Center (NDRC), Ajman University, Ajman, UAE
E-mail: mohana.muthuvalu@utp.edu.my

**Received:** 10 August 2025; **Revised:** 17 November 2025; **Accepted:** 20 November 2025

**Abstract:** This study presents the application of the 2-Point Block Arithmetic Mean (2-BLAM) method for solving radiation transport models formulated as first kind Fredholm integral equations. These equations play a crucial role in predicting radiative heat transfer and neutron or photon transport in slab geometries. The proposed approach used a composite closed Newton-Cotes quadrature scheme to discretize the governing model and formulate a dense algebraic system, which is then solved using the 2-BLAM method. Numerical experiments are carried out on model problems inspired by radiative transfer theory to evaluate the method's computational efficiency, convergence rate, and solution accuracy. The results demonstrate that 2-BLAM outperforms existing iterative methods in terms of convergence speed and computational cost, highlighting its potential for use in radiation physics applications.

***Keywords***: radiation transport model, Fredholm integral equation, semi-smooth kernel, Newton-Cotes quadrature, 2-Point Block Arithmetic Mean (2-BLAM)

**MSC:** 45B05, 65D30, 65R20, 65F10

## 1. Introduction

Integral equations of the first kind are widely encountered in various radiation science domains, particularly in modeling radiative heat transfer [1] and particle transport in nuclear systems. These equations arise in solving the linearized Boltzmann transport equation, Radiative Transfer Equation (RTE), and neutron diffusion problems, where the solution depends on the accumulated effect of radiation interactions throughout a domain [2–4]. Their applications span multiple areas, including remote sensing, radiotherapy planning, reactor core analysis, and optical tomography, where accurate modeling of radiation behavior is critical for design and diagnostics. Radiative transfer in optically thick or scattering-dominated media is commonly expressed through such equations, especially when using methods like discrete ordinates, Monte Carlo simulations, or spherical harmonics ($P_N$) expansions. The mathematical modeling of these radiation phenomena often leads to ill-posed problems, particularly when dealing with limited, noisy, or incomplete


DOI: https://doi.org/10.37256/cm.7120268210

data. In such cases, small perturbations in input can cause large deviations in the solution, requiring stable and efficient numerical schemes for practical computation.

Building on these challenges, many radiation transport problems can be modeled as first kind Fredholm integral equation of the form:

$$\int_a^b K(x,\, t)\phi(t)dt = f(x),\; x \in [a,\, b] \tag{1}$$

where $\phi(t)$ is the unknown radiation intensity or particle flux, $K(x,\, t)$ denotes the kernel representing radiation-matter interaction properties such as absorption, emission, and scattering, and $f(x)$ represents observed boundary radiation data or detector responses. In practical radiation transport applications such as radiative heat transfer in layered media, neutron shielding analysis, and photon propagation in biological tissues the kernel often exhibits a semi-smooth or piecewise continuous nature. This semi-smoothness arises due to abrupt transitions in material composition, optical depth, or scattering coefficients, which cause the kernel to be continuous but not fully differentiable across the entire domain. A common example is found in slab geometries, where the kernel typically represents a Green's function that changes form depending on the spatial relationship between the source and observation points [5, 6]. To formalize this, consider the integral operator $\kappa : S \to T$, defined by

$$\kappa(\phi(t)) = \int_a^b K(x,\, t)\phi(t)dt \tag{2}$$

where $\phi(t)$ belongs to a normed space $S$ and the result lies in another normed space $T$.

**Definition 1** [7] Let $\kappa : S \to T$ be an operator from normed space $S$ into a normed space $T$. The equation $\kappa\phi = f$ is called well-posed if $\kappa$ is onto, one to one and the inverse operator $\kappa^{-1} : T \to S$ is continuous. Otherwise, the equation is called ill-posed.

**Definition 2** [8] A kernel $K(x,\, t)$ is called $q$-semi-smooth if

$$K(x,\, t) = \begin{cases} K_1(x,\, t) & \text{if } a \le t \le x \\ \\ K_2(x,\, t) & \text{if } x \le t \le b \end{cases}$$

where $K_{1,\,2}(x,\, t) \in C^q([a,\, b] \times [a,\, b])$ for $q > 1$.

Numerical methods have been extensively developed and applied to solve equation (1), largely due to the limitations of analytical techniques in handling real-world and complex geometries. Typically, when equation (1) is discretized using numerical techniques such as quadrature [9–12] and projection [7, 13, 14] methods, a dense (or full) algebraic system is obtained. However, solving such systems can be excessively costly as the order of the system increases. In large computational systems, it is generally more efficient to employ iterative solvers rather than direct techniques. This is because iterative methods are able to reach an acceptable approximation with comparatively fewer operations, and the gradual procedure helps to limit the accumulation of round-off errors. Furthermore, direct solvers are highly sensitive to ill-conditioning, which frequently occurs in radiation transport problems, and can suffer from significant numerical errors due to floating-point rounding [15].

Among the iterative solvers, the Arithmetic Mean (AM) family of methods has garnered extensive attention due to its balance of simplicity and adaptability across a wide range of linear and nonlinear problems [11, 16, 17]. Researchers have introduced several enhancements to the basic AM method such as block-wise formulations and relaxation schemes to accelerate convergence and improve numerical stability. These refinements make AM methods especially appealing

for large-scale problems involving semi-smooth kernels and ill-posed characteristics. In this work, a variant of the AM methods, namely the 2-Point Block Arithmetic Mean (2-BLAM) method, which is specifically designed to handle block-structured dense systems efficiently is applied to solve equation (1) with semi-smooth kernel. The 2-BLAM approach capitalizes on localized matrix updates within $2 \times 2$ blocks, enhancing stability while maintaining convergence speed. This makes it highly suitable for solving large algebraic systems generated from the discretization of first-kind integral equations with semi-smooth kernels, common in radiation transport problems involving heterogeneous and layered media. The robustness and scalability of the 2-BLAM method offer a practical numerical framework for high-resolution radiation simulations.

The subsequent sections of this paper are arranged as follows. Section 2 provides a detailed explanation on the derivation of the composite closed Newton-Cotes quadrature approximation, specifically employing the composite Simpson's $\frac{1}{3}$ scheme. Section 3 introduces the formulation of the 2-BLAM method, outlining its implementation for solving the resulting dense algebraic system. Section 4 presents numerical experiments that evaluate the performance of the proposed method in comparison with existing iterative techniques. Finally, section 5 concludes the study with key findings and potential directions for future research.

## 2. Composite closed Newton-Cotes quadrature approximation

A reliable numerical approximation of equation (1) is constructed using the composite closed Newton-Cotes quadrature method. In particular, the composite Simpson's $\frac{1}{3}$ scheme is applied for its favorable balance between computational efficiency and numerical accuracy. The integral domain $[a,\ b]$ is uniformly partitioned into $N$ subintervals, defining the discrete grid points as $x_i = a + ih$ and $t_j = a + jh$, with the uniform step size given by:

$$h = \frac{b-a}{N}. \tag{3}$$

For notational simplicity, the following definitions are introduced:

$$\left.\begin{aligned} K_{i,\ j} &= K\left(x_i,\ t_j\right) \\ \hat{\phi}_j &= \hat{\phi}\left(t_j\right) \\ f_i &= f\left(x_i\right) \end{aligned}\right\}. \tag{4}$$

According to Muthuvalu and Sulaiman [11], applying the composite Simpson's $\frac{1}{3}$ scheme to equation (1) leads to the discretized form:

$$\sum_{j=0}^{N} w_j K_{i,\ j} \hat{\phi}_j = f_i,\ i = 0,\ 1,\ 2,\ \cdots,\ N-2,\ N-1,\ N \tag{5}$$

where $\hat{\phi}$ is the numerical approximation of the unknown function $\phi$, and $w_j$ are the corresponding quadrature weights. Moreover, this discretized form can be compactly represented in matrix form as:

$$A\hat{\phi} = f,\ A \in \mathbb{R}^{(N+1)\times(N+1)},\ \hat{\phi},\ f \in \mathbb{R}^{N+1} \tag{6}$$

where $A$ is the full coefficient matrix formed by weighted kernel values

$$A = \begin{bmatrix} w_0K_{0,\,0} & w_1K_{0,\,1} & \cdots & w_{N-1}K_{0,\,N-1} & w_NK_{0,\,N} \\ w_0K_{1,\,0} & w_1K_{1,\,1} & \cdots & w_{N-1}K_{1,\,N-1} & w_NK_{1,\,N} \\ \vdots & \vdots & \ddots & \vdots & \vdots \\ w_0K_{N-1,\,0} & w_1K_{N-1,\,1} & \cdots & w_{N-1}K_{N-1,\,N-1} & w_NK_{N-1,\,N} \\ w_0K_{N,\,0} & w_1K_{N,\,1} & \cdots & w_{N-1}K_{N,\,N-1} & w_NK_{N,\,N} \end{bmatrix}_{(N+1)\times(N+1)},$$

$$\hat{\phi} = \begin{bmatrix} \hat{\phi}_0 \\ \hat{\phi}_1 \\ \vdots \\ \hat{\phi}_{N-1} \\ \hat{\phi}_N \end{bmatrix} \text{ and } f = \begin{bmatrix} f_0 \\ f_1 \\ \vdots \\ f_{N-1} \\ f_N \end{bmatrix}.$$

The weights, $w_j$ for the composite Simpson's $\frac{1}{3}$ scheme adhere to the relation given below:

$$w_j = \begin{cases} \frac{1}{3}h, & j = 0,\ N \\ \frac{4}{3}h, & j = 1,\ 3,\ 5,\ \cdots,\ N-1 \\ \frac{2}{3}h, & \text{otherwise.} \end{cases} \tag{7}$$

The kernel $K(x,\ t)$ is continuous but only piecewise differentiable, with bounded jumps in its first derivatives across the interface $t = x$. In this implementation, the composite Simpson's $\frac{1}{3}$ scheme is applied on a uniform grid without enforcing panel alignment at the interface. Consequently, the discontinuity may fall inside quadrature panels, placing the integrand in the class of semi-smooth, piecewise-$C^2$ functions. Under these conditions, the discretization remains consistent and stable.

## 3. Block Arithmetic Mean iterative method

This section describes the implementation of the 2-BLAM method for solving the dense system defined in equation (6). The 2-BLAM method is an advanced iterative scheme that updates two independent solution vectors, $\hat{\phi}^1$ and $\hat{\phi}^2$, during each iteration cycle. The coefficient matrix, $A$ is partitioned such that its diagonal elements are grouped into non-singular block $2 \times 2$ submatrices. Further discussions regarding the 2-BLAM method are limited to cases where $N$ is even, resulting in an incomplete block with one ungrouped element. Further development of the 2-BLAM method requires partitioned matrix $A$ into structured submatrices $H_{i,\,j}$ and $H^*_{i,\,j}$ as follows:

$$A = \begin{bmatrix} H_{0,\,0} & H_{0,\,2} & H_{0,\,4} & \cdots & H_{0,\,N-4} & H_{0,\,N-2} & H_{0,\,N} \\ H_{2,\,0} & H_{2,\,2} & H_{2,\,4} & \cdots & H_{2,\,N-4} & H_{2,\,N-2} & H_{2,\,N} \\ H_{4,\,0} & H_{4,\,2} & H_{4,\,4} & \cdots & H_{4,\,N-4} & H_{4,\,N-2} & H_{4,\,N} \\ \vdots & \vdots & \vdots & \ddots & \vdots & \vdots & \vdots \\ H_{N-4,\,0} & H_{N-4,\,2} & H_{N-4,\,4} & \cdots & H_{N-4,\,N-4} & H_{N-4,\,N-2} & H_{N-4,\,N} \\ H_{N-2,\,0} & H_{N-2,\,2} & H_{N-2,\,4} & \cdots & H_{N-2,\,N-4} & H_{N-2,\,N-2} & H_{N-2,\,N} \\ H_{N,\,0} & H_{N,\,2} & H_{N,\,4} & \cdots & H_{N,\,N-4} & H_{N,\,N-2} & H_{N,\,N} \end{bmatrix} \tag{8}$$

and

$$A = \begin{bmatrix} H^*_{0,\,0} & H^*_{0,\,2} & H^*_{0,\,4} & \cdots & H^*_{0,\,N-4} & H^*_{0,\,N-2} & H^*_{0,\,N} \\ H^*_{2,\,0} & H^*_{2,\,2} & H^*_{2,\,4} & \cdots & H^*_{2,\,N-4} & H^*_{2,\,N-2} & H^*_{2,\,N} \\ H^*_{4,\,0} & H^*_{4,\,2} & H^*_{4,\,4} & \cdots & H^*_{4,\,N-4} & H^*_{4,\,N-2} & H^*_{4,\,N} \\ \vdots & \vdots & \vdots & \ddots & \vdots & \vdots & \vdots \\ H^*_{N-4,\,0} & H^*_{N-4,\,2} & H^*_{N-4,\,4} & \cdots & H^*_{N-4,\,N-4} & H^*_{N-4,\,N-2} & H^*_{N-4,\,N} \\ H^*_{N-2,\,0} & H^*_{N-2,\,2} & H^*_{N-2,\,4} & \cdots & H^*_{N-2,\,N-4} & H^*_{N-2,\,N-2} & H^*_{N-2,\,N} \\ H^*_{N,\,0} & H^*_{N,\,2} & H^*_{N,\,4} & \cdots & H^*_{N,\,N-4} & H^*_{N,\,N-2} & H^*_{N,\,N} \end{bmatrix} \tag{9}$$

where notations of $H_{i,\,j}$ and $H^*_{i,\,j}$ are defined as follows

$$H_{i,\,j} = \begin{bmatrix} w_j K_{i,\,j} & w_{j+1} K_{i,\,j+1} \\ w_j K_{i+1,\,j} & w_{j+1} K_{i+1,\,j+1} \end{bmatrix} \tag{10}$$

and

$$H^*_{i,\,j} = \begin{bmatrix} w_{j-1} K_{i-1,\,j-1} & w_j K_{i-1,\,j} \\ w_{j-1} K_{i,\,j-1} & w_j K_{i,\,j} \end{bmatrix} \tag{11}$$

respectively. Based on matrices (8) and (9), it is noticeable that $H_{N,\,N} = w_N K_{N,\,N}$ and $H^*_{0,\,0} = w_0 K_{0,\,0}$. Meanwhile, $H_{N,\,j}$ $(j = 0,\ 2,\ 4,\ \cdots,\ N-4,\ N-2)$ and $H^*_{0,\,j}$ $(j = 2,\ 4,\ \cdots N-4,\ N-2,\ N)$ are row vector of order 2. Whereas $H_{i,\,N}$ $(i = 0,\ 2,\ 4,\ \cdots,\ N-4,\ N-2)$ and $H^*_{i,\,0}$ $(i = 2,\ 4,\ \cdots,\ N-4,\ N-2,\ N)$ are a column vector of order 2.

Now, matrices in equations (8) and (9) provide the structural basis for the two-matrix splitting:

$$A = D_1 - L_1 - U_1 \tag{12}$$

and

$$A = D_2 - L_2 - U_2. \tag{13}$$

Using equations (8) and (12), the splitting of $D_1,\ -L_1$ and $-U_1$ can be expressed as follows:

$$D_1 = \begin{bmatrix} H_{0,\,0} & & & & & & \\ & H_{2,\,2} & & & & & \\ & & H_{4,\,4} & & 0 & & \\ & & & \ddots & & & \\ & & 0 & & H_{N-4,\,N-4} & & \\ & & & & & H_{N-2,\,N-2} & \\ & & & & & & H_{N,\,N} \end{bmatrix}, \tag{14}$$

$$-L_1 = \begin{bmatrix} & & & & & & \\ H_{2,\,0} & & & & & & \\ H_{4,\,0} & H_{4,\,2} & & & 0 & & \\ \vdots & \vdots & \ddots & & & & \\ H_{N-4,\,0} & H_{N-4,\,2} & \cdots & H_{N-4,\,N-6} & & & \\ H_{N-2,\,0} & H_{N-2,\,2} & \cdots & H_{N-2,\,N-6} & H_{N-2,\,N-4} & & \\ H_{N,\,0} & H_{N,\,2} & \cdots & H_{N,\,N-6} & H_{N,\,N-4} & H_{N,\,N-2} & \end{bmatrix} \tag{15}$$

and

$$-U_1 = \begin{bmatrix} H_{0,\,2} & H_{0,\,4} & H_{0,\,6} & \cdots & H_{0,\,N-2} & H_{0,\,N} \\ & H_{2,\,4} & H_{2,\,6} & \cdots & H_{2,\,N-2} & H_{2,\,N} \\ & & H_{4,\,6} & \cdots & H_{4,\,N-2} & H_{4,\,N} \\ & & & \ddots & \vdots & \vdots \\ & 0 & & & H_{N-4,\,N-2} & H_{N-4,\,N} \\ & & & & & H_{N-2,\,N} \\ & & & & & \end{bmatrix} \tag{16}$$

respectively. Following the same splitting strategy as employed for the first matrix splitting, the components $D_2$, $-L_2$ and $-U_2$ are constructed as described in equations (9) and (13).

$$D_2 = \begin{bmatrix} H^*_{0,\,0} & & & & & & \\ & H^*_{2,\,2} & & & & & \\ & & H^*_{4,\,4} & & 0 & & \\ & & & \ddots & & & \\ & & 0 & & H^*_{N-4,\,N-4} & & \\ & & & & & H^*_{N-2,\,N-2} & \\ & & & & & & H^*_{N,\,N} \end{bmatrix}, \tag{17}$$

$$-L_2 = \begin{bmatrix} & & & & & \\ H^*_{2,\,0} & & & & & \\ H^*_{4,\,0} & H^*_{4,\,2} & & & 0 & \\ \vdots & \vdots & \ddots & & & \\ H^*_{N-4,\,0} & H^*_{N-4,\,2} & \cdots & H^*_{N-4,\,N-6} & & \\ H^*_{N-2,\,0} & H^*_{N-2,\,2} & \cdots & H^*_{N-2,\,N-6} & H^*_{N-2,\,N-4} & \\ H^*_{N,\,0} & H^*_{N,\,2} & \cdots & H^*_{N,\,N-6} & H^*_{N,\,N-4} & H^*_{N,\,N-2} \end{bmatrix} \tag{18}$$

and

$$-U_2 = \begin{bmatrix} H^*_{0,\,2} & H^*_{0,\,4} & H^*_{0,\,6} & \cdots & H^*_{0,\,N-2} & H^*_{0,\,N} \\ & H^*_{2,\,4} & H^*_{2,\,6} & \cdots & H^*_{2,\,N-2} & H^*_{2,\,N} \\ & & H^*_{4,\,6} & \cdots & H^*_{4,\,N-2} & H^*_{4,\,N} \\ & & & \ddots & \vdots & \vdots \\ & 0 & & & H^*_{N-4,\,N-2} & H^*_{N-4,\,N} \\ & & & & & H^*_{N-2,\,N} \\ & & & & & \end{bmatrix} \tag{19}$$

respectively.

Thus, for non-singular $(D_1 - \omega L_1)$ and $(D_2 - \omega U_2)$ matrices, the general formulation for 2-BLAM iterative method is defines as

$$\left.\begin{aligned} (D_1 - \omega L_1)\,\hat{\phi}^1 &= [(1-\omega)D_1 + \omega U_1]\,\hat{\phi}^{(k)} + \omega f \\ (D_2 - \omega U_2)\,\hat{\phi}^2 &= [(1-\omega)D_2 + \omega L_2]\,\hat{\phi}^{(k)} + \omega f \\ \hat{\phi}^{(k+1)} &= \frac{\hat{\phi}^1 + \hat{\phi}^2}{2} \end{aligned}\right\} \tag{20}$$

where $\omega$ denotes the acceleration parameter. By applying formula (20), computational procedure for 2-BLAM method associated with composite Simpson's $\frac{1}{3}$ scheme to solve problem (1) is explained in Algorithm 1. Throughout the iteration process, the Lower-Upper (LU) decomposition method employing the Crout technique will be utilized to compute the values of $\hat{\phi}^1$ and $\hat{\phi}^2$ for each block ($H_{i,\,i}$ and $H^*_{i,\,i}$). By employing the Crout technique, the following formulations are used to calculate $\hat{\phi}^1_{i+1}$, $\hat{\phi}^1_i$, $\hat{\phi}^2_i$ and $\hat{\phi}^2_{i-1}$:

$$\hat{\phi}^1_{i+1} = \frac{S^1_{i+1} - (w_i K_{i+1,\,i})\left(\dfrac{S^1_i}{w_i K_{i,\,i}}\right)}{(w_{i+1}K_{i+1,\,i+1}) - (w_i K_{i+1,\,i})\left(\dfrac{w_{i+1}K_{i,\,i+1}}{w_i K_{i,\,i}}\right)} \tag{21}$$

$$\hat{\phi}_i^1 = \frac{S_i^1}{w_i K_{i,\,i}} - \frac{w_{i+1} K_{i,\,i+1}}{w_i K_{i,\,i}} \hat{\phi}_{i+1}^1 \tag{22}$$

$$\hat{\phi}_i^2 = \frac{S_i^2 - (w_{i-1} K_{i,\,i-1}) \left( \dfrac{S_{i-1}^2}{w_{i-1} K_{i-1,\,i-1}} \right)}{(w_i K_{i,\,i}) - (w_{i-1} K_{i,\,i-1}) \left( \dfrac{w_i K_{i-1,\,i}}{w_{i-1} K_{i-1,\,i-1}} \right)} \tag{23}$$

and

$$\hat{\phi}_{i-1}^2 = \frac{S_{i-1}^2}{w_{i-1} K_{i-1,\,i-1}} - \frac{w_i K_{i-1,\,i}}{w_{i-1} K_{i-1,\,i-1}} \hat{\phi}_i^2 \tag{24}$$

respectively, where

$$s_i^1 = f_i - \sum_{j=0}^{i-1} w_j K_{i,\,j} \hat{\phi}_j^1 - \sum_{j=i+2}^{N} w_j K_{i,\,j} \hat{\phi}_j^{(k)},$$

$$s_{i+1}^1 = f_{i+1} - \sum_{j=0}^{i-1} w_j K_{i+1,\,j} \hat{\phi}_j^1 - \sum_{j=i+2}^{N} w_j K_{i+1,\,j} \hat{\phi}_j^{(k)},$$

$$s_{i-1}^2 = f_{i-1} - \sum_{j=0}^{i-2} w_j K_{i-1,\,j} \hat{\phi}_j^{(k)} - \sum_{j=i+1}^{N} w_j K_{i-1,\,j} \hat{\phi}_j^2,$$

$$s_i^2 = f_i - \sum_{j=0}^{i-2} w_j K_{i,\,j} \hat{\phi}_j^{(k)} - \sum_{j=i+1}^{N} w_j K_{i,\,j} \hat{\phi}_j^2,$$

$$S_i^1 = (1-\omega) \left[ w_i K_{i,\,i} \hat{\phi}_i^{(k)} + w_{i+1} K_{i,\,i+1} \hat{\phi}_{i+1}^{(k)} \right] + \omega \left( s_i^1 \right),$$

$$S_{i+1}^1 = (1-\omega) \left[ w_i K_{i+1,\,i} \hat{\phi}_i^{(k)} + w_{i+1} K_{i+1,\,i+1} \hat{\phi}_{i+1}^{(k)} \right] + \omega \left( s_{i+1}^1 \right),$$

$$S_{i-1}^2 = (1-\omega) \left[ w_{i-1} K_{i-1,\,i-1} \hat{\phi}_{i-1}^{(k)} + w_i K_{i-1,\,i} \hat{\phi}_i^{(k)} \right] + \omega \left( s_{i-1}^2 \right),$$

and

$$S_i^2 = (1-\omega) \left[ w_{i-1} K_{i,\,i-1} \hat{\phi}_{i-1}^{(k)} + w_i K_{i,\,i} \hat{\phi}_i^{(k)} \right] + \omega \left( s_i^2 \right).$$

For the ungrouped point, the standard AM point-based iteration described in Muthuvalu and Sulaiman [11] is employed. In the radiation transport problems considered, the kernel $K(x,\ t)$ represents semi-smooth but non-singular physical interactions (e.g., absorption or scattering coefficients) that remain finite and non-zero along the diagonal, i.e., $K_{i,\ i} \neq 0$ for all $i$. Therefore, the denominator in equations (21)-(24) does not encounter a division-by-zero condition under the assumed problem class. During implementation, $\hat{\phi}_{i+1}^{1}$ and $\hat{\phi}_{i}^{2}$ are first computed using equations (21) and (23), respectively. The obtained values are then substituted into equations (22) and (24) to evaluate $\hat{\phi}_{i}^{1}$ and $\hat{\phi}_{i-1}^{2}$ within each iteration cycle.

**Algorithm 1** 2-BLAM algorithm

(i) Set $\hat{\phi}^{(0)} = \hat{\phi}^{1} = \hat{\phi}^{2} = 0,\ \varepsilon$

(ii) Iteration cycle

Stage 1

Level 1

**for** $i = 0,\ 2,\ 4,\ \cdots,\ N-4,\ N-2$

Compute $\begin{bmatrix} \hat{\phi}_i \\ \hat{\phi}_{i+1} \end{bmatrix}^{1} \leftarrow H_{i,\ i}^{-1} \left[ (1-\omega) H_{i,\ i} \begin{bmatrix} \hat{\phi}_i \\ \hat{\phi}_{i+1} \end{bmatrix}^{(k)} + \omega \begin{bmatrix} s_i \\ s_{i+1} \end{bmatrix}^{1} \right]$

**for** $i = N$

Compute $\hat{\phi}_{N}^{1} \leftarrow (1-\omega)\hat{\phi}_{N}^{(k)} + \dfrac{\omega}{w_N K_{N,\ N}} \left[ f_N - \sum_{j=0}^{N-1} w_j K_{N,\ j} \hat{\phi}_{j}^{1} \right]$

Level 2

**for** $i = N,\ N-2,\ N-4,\ \cdots,\ 4,\ 2$

Compute $\begin{bmatrix} \hat{\phi}_{i-1} \\ \hat{\phi}_i \end{bmatrix}^{2} \leftarrow \left( H_{i,\ i}^{*} \right)^{-1} \left[ (1-\omega) H_{i,\ i}^{*} \begin{bmatrix} \hat{\phi}_{i-1} \\ \hat{\phi}_i \end{bmatrix}^{(k)} + \omega \begin{bmatrix} s_{i-1} \\ s_i \end{bmatrix}^{2} \right]$

**for** $i = 0$

Compute $\hat{\phi}_{0}^{2} \leftarrow (1-\omega)\hat{\phi}_{0}^{(k)} + \dfrac{\omega}{w_0 K_{0,\ 0}} \left[ f_0 - \sum_{j=1}^{N} w_j K_{0,\ j} \hat{\phi}_{j}^{2} \right]$

Stage 2

**for** $i = 0,\ 1,\ 2,\ \cdots,\ N-2,\ N-1,\ N$

Compute $\hat{\phi}_{i}^{(k+1)} \leftarrow \dfrac{\hat{\phi}_{i}^{1} + \hat{\phi}_{i}^{2}}{2}.$

(iii) Convergence test. If the maximum norm, $\left\| \hat{\phi}_{i}^{(k+1)} - \hat{\phi}_{i}^{(k)} \right\| \leq \varepsilon$ (with $\varepsilon$ as the prescribed tolerance) is satisfied, proceed to Step (iv); otherwise, return to Step (ii) and repeat the iteration.

(iv) Stop.

The 2-BLAM method utilizes a two-sided splitting approach and the iterative formulation of the 2-BLAM method is defined as

$$\hat{\phi}^{(k+1)} = (1-\omega)\hat{\phi}^{(k)} + \frac{\omega}{2} \left[ (D_1 - L_1)^{-1} U_1 + (D_2 - U_2)^{-1} L_2 \right] \hat{\phi}^{(k)} + \frac{\omega}{2} \left[ (D_1 - L_1)^{-1} + (D_2 - U_2)^{-1} \right] f \tag{25}$$

where $\omega \in (0,\ 2)$. The corresponding iteration matrix is

$$T_{2-\mathrm{BLAM}} = (1-\omega) I + \frac{\omega}{2} \left[ (D_1 - L_1)^{-1} U_1 + (D_2 - U_2)^{-1} L_2 \right]. \tag{26}$$

The matrices $(D_1 - L_1)$ and $(D_2 - U_2)$ are invertible under the assumed problem class, as the discretization of the semi-smooth kernel $K(x,\ t)$ yields a strictly diagonally dominant matrix with positive quadrature weights $(w_j > 0)$ and

bounded kernel values on $[a,\ b] \times [a,\ b]$. Hence, each diagonal block of $D_1$ and $D_2$ remains non-singular, ensuring the existence of $(D_1 - L_1)^{-1}$ and $(D_2 - U_2)^{-1}$.

**Theorem 1** (Convergence condition of the 2-BLAM method)

Let $A$ be a non-singular matrix with the block splittings described in equations (12)-(19). The 2-BLAM iterative method converges for any initial guess $\hat{\phi}^{(0)}$ to the solution of the system $A\hat{\phi} = f$, provided that the spectral radius of the iteration matrix satisfies

$$\rho\left(T_{2-\mathrm{BLAM}}\right) < 1.$$

**Proof.** The 2-BLAM iteration is of the form

$$\hat{\phi}^{(k+1)} = T_{2-\mathrm{BLAM}}\hat{\phi}^{(k)} + g$$

where $g = \dfrac{\omega}{2}\left[(D_1 - L_1)^{-1} + (D_2 - U_2)^{-1}\right] f$ and this is a linear fixed-point iteration. Now, let $\hat{\phi}^*$ be any fixed point i.e.

$$\hat{\phi}^* = T_{2-\mathrm{BLAM}}\hat{\phi}^* + g$$

and the error

$$e^{(k)} = \hat{\phi}^{(k)} - \hat{\phi}^*.$$

Subtracting the fixed-point identity from the iteration yields the homogeneous recursion

$$e^{(k+1)} = T_{2-\mathrm{BLAM}}e^{(k)}.$$

By induction,

$$e^{(k)} = T^k_{2-\mathrm{BLAM}}e^{(0)} (k \geq 0).$$

The convergence of the iteration is characterized exactly by the spectral radius of the iteration matrix, $\rho\left(T_{2-\mathrm{BLAM}}\right)$. In particular,

• If $\rho\left(T_{2-\mathrm{BLAM}}\right) < 1$, then every eigenvalue $\lambda$ of $T_{2-\mathrm{BLAM}}$ satisfies $|\lambda| < 1$. Hence $T^k_{2-\mathrm{BLAM}} \to 0$ as $k \to \infty$, so $e^{(k)} \to 0$ for every initial error $e^{(0)}$. Therefore $\hat{\phi}^{(k)} \to \hat{\phi}^*$, furthermore $I - T_{2-\mathrm{BLAM}}$ is invertible and the fixed point is unique, given by $\hat{\phi}^* = \left(I - T_{2-\mathrm{BLAM}}\right)^{-1} g$.

• Conversely, if the iteration converges to a limit for every initial $\hat{\phi}^{(0)}$, then for every $e^{(0)}$ we must have $T^k_{2-\mathrm{BLAM}}e^{(0)} \to 0$ and this can occur only when $\rho\left(T_{2-\mathrm{BLAM}}\right) < 1$. If $\rho\left(T_{2-\mathrm{BLAM}}\right) \geq 1$, there exists an eigenvalue $\lambda$ with $|\lambda| \geq 1$, and one may choose an initial error in the corresponding (generalised) eigenspace for which $T^k_{2-\ \mathrm{BLAM}}\, e^{(0)}$ does not converge to zero, contradicting universal convergence.

Thus, the iteration converges for every initial guess if and only if $\rho\left(T_{2-\mathrm{BLAM}}\right) < 1$. □

**Theorem 2** (Stability of the 2-BLAM method)

Suppose the spectral radius of the iteration matrix satisfies $\rho\left(T_{2-\mathrm{BLAM}}\right)<1$, then the 2-BLAM method is stable with respect to perturbations in the right-hand side $f$ and the propagated error remains bounded.

**Proof.** Let the actual system be

$$A\hat{\phi}=f$$

and the perturbed system be

$$A\widetilde{\phi}=f+\delta f,$$

where $\delta f$ is a small perturbation in the right-hand side.

Let $\hat{\phi}^{(k)}$ and $\widetilde{\phi}^{(k)}$ denote the iterates generated by the 2-BLAM method for the unperturbed and perturbed systems, respectively. The 2-BLAM iterative scheme applied to each system yields

$$\hat{\phi}^{(k+1)}=T_{2-\mathrm{BLAM}}\hat{\phi}^{(k)}+g$$

and

$$\widetilde{\phi}^{(k+1)}=T_{2-\mathrm{BLAM}}\widetilde{\phi}^{(k)}+\widetilde{g}$$

where

$$g=\frac{\omega}{2}\left[(D_1-L_1)^{-1}+(D_2-U_2)^{-1}\right]f$$

and

$$\widetilde{g}=\frac{\omega}{2}\left[(D_1-L_1)^{-1}+(D_2-U_2)^{-1}\right](f+\delta f).$$

Define the error due to perturbation as $e^{(k)}=\widetilde{\phi}^{(k)}-\hat{\phi}^{(k)}$ and by subtracting the two update equations gives

$$e^{(k+1)}=T_{2-\mathrm{BLAM}}e^{(k)}+\delta g,$$

where

$$\delta g=\tilde{g}-g=\frac{\omega}{2}\left[(D_1-L_1)^{-1}+(D_2-U_2)^{-1}\right]\delta f.$$

and closed form by induction is

$$e^{(k)} = T_{2-\mathrm{BLAM}}^{k} e^{(0)} + \sum_{j=0}^{k-1} T_{2-\mathrm{BLAM}}^{j} \delta g.$$

If $\rho\left(T_{2-\mathrm{BLAM}}\right) < 1$ then $T_{2-\mathrm{BLAM}}^{k} \to 0$ and the geometric series converges in operator norm so the iterates have the limit

$$\lim_{k\to\infty} e^{(k)} = \left(I - T_{2-\mathrm{BLAM}}\right)^{-1} \delta g.$$

Therefore, the asymptotic perturbation is bounded by the resolvent of $T_{2-\ \mathrm{BLAM}}$

$$\limsup_{k\to\infty} \left\| e^{(k)} \right\| \leq \left\| \left(I - T_{2-\mathrm{BLAM}}\right)^{-1} \right\| \|\delta g\| \leq \frac{\|\delta g\|}{1 - \rho\left(T_{2-\mathrm{BLAM}}\right)}.$$

Hence, the propagated perturbation remains bounded, confirming that the 2-BLAM method is stable with respect to small changes in the input data. □

To assess the computational complexity of the proposed 2-BLAM method, the arithmetic operations required to solve problem (1) were estimated based on the operations executed per iteration. In this analysis, it is assumed that all coefficients and matrix elements in system (6) are precomputed and stored prior to iteration. The abbreviations ADD/SUB and MUL/DIV denote Addition/Subtraction (ADD/SUB) and Multiplication/Division (MUL/DIV) operations, respectively. According to Algorithm 1, the total number of arithmetic operations per iteration (excluding the convergence test) for the 2-BLAM method can be expressed as

$$\left(2N^2 + 10N + 3\right) \text{ ADD/SUB } + \left(2N^2 + 17N + 7\right) \text{ MUL/DIV.}$$

These expressions indicate that the arithmetic effort per iteration is dominated by $O\left(N^2\right)$ terms arising from dense block-matrix multiplications and updates. Consequently, the asymptotic computational complexity of a single iteration is $O\left(N^2\right)$, while the total cost of the method scales as $O\left(kN^2\right)$, where $k$ is the number of iterations required for convergence.

## 4. Numerical simulations

This section presents the numerical results to evaluate the effectiveness of the 2-BLAM iterative method in solving equation (1), which is relevant to radiation transport applications. These problems include features like semi-smooth kernels, which are common in radiation-related integral formulations and often present challenges for conventional iterative solvers. For comparative purposes, the performance of the 2-BLAM method is compared with the standard Gauss-Seidel (GS), Block Gauss-Seidel (BGS) and AM methods. The convergence behavior is assessed based on the number of iterations and total computational time required to reach a predefined error tolerance of $\varepsilon = 10^{-10}$. All simulations are performed on a system equipped with an Intel (R) Core (TM) 2 CPU @ 1.66 GHz, with the algorithms implemented in the *C* programming language. The experiments are conducted for various values of $N$, and the relaxation parameter $\omega$ is optimized by executing the 2-BLAM algorithm across a range of $\omega$ values. The optimal $\omega$ is selected as the value that yields the minimum number of iterations (within a range of $\pm$ 0.01).

**Test Problem 1** The Fredholm integral equation of the first kind

$$\int_0^1 K(x,\, t)\phi(t)dt = \frac{x^3 - x}{6} \tag{27}$$

with the kernel defined as

$$K(x,\, t) = \begin{cases} t(x-1), & t < x \\ x(t-1), & x \leq t \end{cases} \tag{28}$$

arises in the study of radiative transfer within a one-dimensional slab of participating media, such as gases or semi-transparent solids, where radiation interacts with the medium through absorption, emission, and possibly scattering. In this formulation, $\phi(t)$ represents the unknown source function or radiative intensity distribution at location $t$. The kernel $K(x,\, t)$ characterizes the interaction between radiation emitted at position $t$ and its contribution to the radiative energy at position $x$, considering the geometry and boundary effects. The piecewise-defined kernel reflects the asymmetry in radiation transfer, depending on whether $t < x$ (radiation reaching $x$ from a location to the left) or $t \geq x$ (from the right). The right-hand side can be interpreted as a known source term or a resultant net radiative flux, possibly derived from energy balance or experimental data. The exact solution to this test problem 1 is known to be

$$\phi(x) = x \tag{29}$$

which may correspond to a linearly varying radiative intensity, consistent with simple radiative diffusion models under specific boundary conditions. The numerical results for test problem 1 are presented in Table 1 and illustrated in Figures 1 and 2.

**Table 1.** Numerical results for test problem 1

| Parameter | Methods | $N$ | | | | | |
|---|---|---|---|---|---|---|---|
| | | 240 | 480 | 960 | 1, 920 | 3, 840 | 7,680 |
| Number of iterations | GS | 305 | 380 | 461 | 551 | 647 | 755 |
| | BGS | 247 | 293 | 345 | 419 | 463 | 568 |
| | AM | 136 | 140 | 143 | 144 | 162 | 222 |
| | 2-BLAM | 31 | 31 | 32 | 32 | 33 | 33 |
| Computational time (in seconds) | GS | 5.30 | 16.74 | 68.47 | 236.40 | 811.43 | 2,344.30 |
| | BGS | 4.89 | 13.68 | 56.11 | 205.04 | 635.89 | 2,004.28 |
| | AM | 4.24 | 12.50 | 50.10 | 186.33 | 544.14 | 1,615.30 |
| | 2-BLAM | 1.20 | 2.95 | 16.03 | 61.10 | 153.40 | 335.11 |

Figure 1 compares the radiative intensity profiles obtained using the 2-BLAM method for $N = 240$ and $N = 7,680$ grid resolutions against the exact solution. The results show that as the grid is refined, the numerical solution produced by 2-BLAM approaches the exact profile, demonstrating improved accuracy and convergence with increasing $N$. The close agreement at higher resolution confirms the consistency and stability of the 2-BLAM scheme for solving radiative transfer problems.

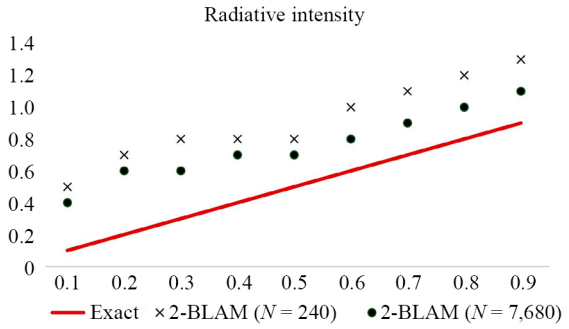


**Figure 1.** Radiative intensity profiles obtained using the 2-BLAM method for $N = 240$ and $N = 7,680$ (for test problem 1)

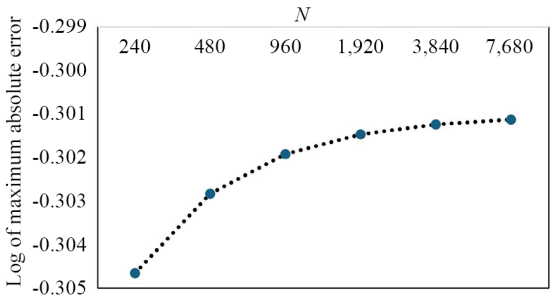


**Figure 2.** Log of maximum absolute error by using 2-BLAM method for test problem 1

Figure 2 presents the logarithmic variation of the maximum absolute error obtained using the 2-BLAM method across different grid sizes $N$. The error remains nearly constant as $N$ increases, indicating that the 2-BLAM method maintains consistent numerical accuracy and stability with mesh refinement.

**Test Problem 2** The Fredholm integral equation of the first kind

$$\int_0^1 K(x,\, t)\phi(t)dt = e^x + (1-e)x - 1 \tag{30}$$

with the kernel

$$K(x,\, t) = \begin{cases} t(x-1), & t \le x \\ x(t-1), & x < t \end{cases} \tag{31}$$

can be modeled as a boundary-influenced radiative heat transfer problem in a non-isothermal slab, where the radiation within the medium is driven by spatially varying internal sources and non-uniform boundary conditions. In this scenario, $\phi(t)$ represents the local emissive power or temperature-dependent radiative source strength, which varies with position due to localized heat generation or absorption. The kernel $K(x,\, t)$ captures the spatial influence of radiative contributions from other locations within the slab, modulated by position-dependent geometrical or optical properties. The asymmetry of the kernel reflects the directional bias of radiation within the slab, with $t \le x$ and $t > x$ modeling radiative influence from the left and right, respectively. The non-polynomial right-hand side, could correspond to a prescribed radiative

flux distribution, possibly derived from external heating, boundary irradiation, or experimentally observed flux gradients. Unlike simpler diffusion-based models, this formulation accommodates exponential growth in radiation intensity, as seen in the exact solution

$$\phi(x) = e^{x} \tag{32}$$

indicating strong positional dependence of the source term, a scenario relevant in media exposed to localized laser heating, high-energy particle irradiation, or temperature-sensitive radiative processes. The numerical results for test problem 2 are presented in Table 2 and illustrated in Figures 3 and 4.

**Table 2.** Numerical results for test problem 2

| Parameter | Methods | $N$ | | | | | |
|---|---|---|---|---|---|---|---|
| | | 240 | 480 | 960 | 1,920 | 3,840 | 7,680 |
| Number of iterations | GS | 318 | 397 | 479 | 572 | 668 | 786 |
| | BGS | 251 | 315 | 370 | 438 | 511 | 592 |
| | AM | 141 | 146 | 148 | 149 | 169 | 231 |
| | 2-BLAM | 34 | 34 | 35 | 35 | 35 | 35 |
| Computational time (in seconds) | GS | 6.42 | 18.13 | 70.15 | 266.75 | 877.30 | 2,470.18 |
| | BGS | 5.82 | 15.11 | 61.09 | 224.27 | 714.23 | 2,056.63 |
| | AM | 5.03 | 13.70 | 53.60 | 191.42 | 560.16 | 1,688.30 |
| | 2-BLAM | 1.31 | 3.40 | 17.50 | 64.26 | 165.88 | 370.03 |

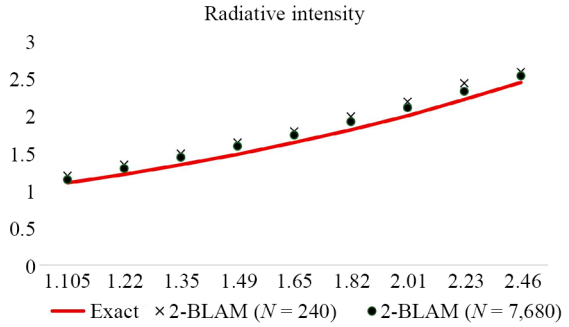


**Figure 3.** Radiative intensity profiles obtained using the 2-BLAM method for $N = 240$ and $N = 7,680$ (for test problem 2)

Figure 3 illustrates the radiative intensity profiles computed using the 2-BLAM method for $N = 240$ and $N = 7,680$ compared with the exact solution. The results show that as the grid resolution increases, the numerical solution closely follows the exact curve, demonstrating improved accuracy and convergence of the 2-BLAM method. The good agreement across all data points confirms the stability and reliability of the proposed approach for radiative transfer analysis.

Figure 4 presents the logarithmic variation of the maximum absolute error with respect to the grid size $N$ for the 2-BLAM method. The results show a slight reduction in error magnitude as $N$ increases, indicating consistent convergence behavior. The nearly flat trend at larger $N$ values suggests that the method achieves numerical stability and that the discretization error becomes dominant for finer grids.

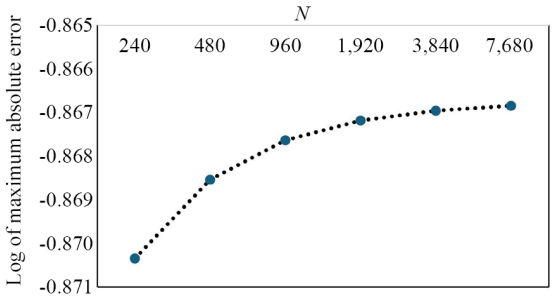


**Figure 4.** Log of maximum absolute error by using 2-BLAM method for test problem 2

Furthermore, Table 3 presented the percentage reduction in both the number of iterations and computational time achieved by the BGS, AM and 2-BLAM methods relative to the GS method. This comparative analysis highlights the computational advantages of the proposed methods, particularly in terms of convergence efficiency and overall runtime, demonstrating their effectiveness in solving Fredholm integral equations of the first kind arising from radiation-related problems.

**Table 3.** Percentage reduction by the BGS, AM and 2-BLAM methods compared to the GS method

| Methods | Number of iterations (%) | | Computational time (%) | |
|---|---|---|---|---|
| | Test Problem 1 | Test Problem 2 | Test Problem 1 | Test Problem 2 |
| BGS | 19.01-28.44 | 21.06-24.69 | 7.73-21.64 | 9.34-18.58 |
| AM | 55.40-74.97 | 55.66-74.71 | 20.00-32.95 | 21.65-36.15 |
| 2-BLAM | 89.83-95.63 | 89.30-95.55 | 74.15-85.71 | 75.05-85.03 |

## 5. Conclusion

This work successfully demonstrated the application and effectiveness of the 2-BLAM iterative method for solving radiation transport models represented by Fredholm integral equations of the first kind with semi-smooth kernels. The numerical experiments conducted on test problems highlight the superior performance of the 2-BLAM method. Specifically, 2-BLAM achieved significantly faster convergence rates and reduced computational time while maintaining solution accuracy. The block-wise update structure and use of LU decomposition via the Crout technique enhance both the numerical stability and efficiency of the method, making it well-suited for large-scale radiation transport simulations in heterogeneous and layered media.

Future research will investigate adaptive block strategies, parallel implementations, and hybrid frameworks incorporating machine learning for automated parameter selection, further extending the applicability of 2-BLAM across computational radiation physics and related fields. Additional work will examine discretization enhancements for semi-smooth kernels, including discontinuity-aware quadrature schemes and interface-aligned panelisation, to better ascertain their influence on operator conditioning and iterative solver performance. As the current study considers a noise-free deterministic setting, explicit regularisation mechanisms such as Tikhonov and related stabilisation techniques are not yet incorporated, and their integration represents a natural and important direction for future research, particularly for inverse problems involving noisy data.

## Acknowledgments

This research was funded by National Collaborative Research Fund (Universiti Teknologi PETRONAS-Universiti Malaysia Pahang) (Cost Center: 015MC0-033) and Ministry of Higher Education under the Fundamental Research Grant Scheme (FRGS/1/2014/SG04/UTP/03/1).

## Conflict of interest

The authors declare that there is no conflict of interest regarding the publication of this paper.

## References

[1] Modest MF. *Radiative Heat Transfer*. 3rd ed. New York: Academic Press; 2013.

[2] Gao M, Shi Y. A modified implicit Monte Carlo method for frequency-dependent three-temperature radiative transfer equations. *Nuclear Science and Engineering*. 2025; 199(2): 325-337.

[3] Jiang YF. An implicit finite volume scheme to solve the time-dependent radiation transport equation based on discrete ordinates. *The Astrophysical Journal Supplement Series*. 2021; 253: 49.

[4] Judd KP, Handler RA. Numerical solution of the radiation transport equation at an air-water interface for a stratified medium. *Frontiers in Mechanical Engineering*. 2019; 5: 1.

[5] Dölz J, Palii O, Schlottbom M. On robustly convergent and efficient iterative methods for anisotropic radiative transfer. *Journal of Scientific Computing*. 2022; 90: 94.

[6] Zhao JM, Liu LH. Solution of radiative heat transfer in graded index media by least square spectral element method. *International Journal of Heat and Mass Transfer*. 2007; 50: 2634-2642.

[7] Maleknejad K, Mollapourasl R, Nouri K. Convergence of numerical solution of the Fredholm integral equation of the first kind with degenerate kernel. *Applied Mathematics and Computation*. 2006; 181(2): 1000-1007.

[8] Kang S, Koltracht I, Rawitscher G. Nyström-Clenshaw-Curtis quadrature for integral equations with discontinuous kernels. *Mathematics of Computation*. 2002; 72(242): 729-756.

[9] Laurie DP. Computation of Gauss-type quadrature formulas. *Journal of Computational and Applied Mathematics*. 2001; 127(1-2): 201-217.

[10] Muthuvalu MS, Noar NAZM, Setiawan H, Kurniawan I, Momani S. Numerical solution of first kind Fredholm integral equations with semi-smooth kernel: A two-stage iterative approach. *Results in Applied Mathematics*. 2024; 24: 100520.

[11] Muthuvalu MS, Sulaiman J. Half-sweep arithmetic mean method with composite trapezoidal scheme for solving linear Fredholm integral equations. *Applied Mathematics and Computation*. 2011; 217(12): 5442-5448.

[12] Muthuvalu MS, Sulaiman J. The arithmetic mean iterative methods for solving dense linear systems arise from first kind linear Fredholm integral equations. *Proceedings of the Romanian Academy, Series A*. 2012; 13(3): 198-206.

[13] Patel S, Panigrahi BL, Nelakanti G. Legendre spectral projection methods for Fredholm integral equations of the first kind. *Journal of Inverse and Ill-Posed Problems*. 2022; 30(5): 677-691.

[14] Patel S, Panigrahi BL. Jacobi spectral projection methods for Fredholm integral equations of the first kind. *Numerical Algorithms*. 2024; 96: 33-57.

[15] Dias JMB, Leitão JMN. Group lapped iterative technique for fast solution of large linear systems. In: *Proceedings of the IEEE International Conference on Electronics, Circuits and Systems*. New York: IEEE; 1998. p.531-534.

[16] Aruchunan E, Chew JVL, Muthuvalu MS, Sunarto A, Sulaiman J. A Newton-Modified Weighted Arithmetic Mean solution of nonlinear porous medium type equations. *Symmetry*. 2021; 13(8): 1511.

[17] Galligani E. The arithmetic mean method for solving systems of nonlinear equations in finite differences. *Applied Mathematics and Computation*. 2006; 181(1): 579-597.